3-25-2018

Topographic Control on Post-LGM Groundings of the West Antarctic Ice Sheet in the Whales Deep Basin, Eastern Ross Sea

Matthew Danielson
Louisiana State University and Agricultural and Mechanical College

TOPOGRAPHIC CONTROL ON POST-LGM GROUNDINGS OF THE WEST ANTARCTIC ICE SHEET IN THE WHALES DEEP BASIN, EASTERN ROSS SEA

A Thesis

Submitted to the Graduate Faculty of
Louisiana State University
Agricultural and Mechanical College
In the partial fulfillment of the
requirements for the degree of
Master in Science

In

The Department of Geology and Geophysics

by
Matthew Danielson
B.S., Texas A&M, 2015
May 2018

TABLE OF CONTENTS

ABSTRACT

By the peak of the Last Glacial Maximum (LGM), the West Antarctic Ice Sheet (WAIS) had advanced to the outer continental shelf of eastern Ross Sea trough basins. During the post-LGM retreat, the WAIS paused several times within 75 km of the Whales Deep Basin (WDB) shelf edge. An overlapping stack of seven grounding zone wedges (GZWs) records the locations of these groundings. Here we used ~7500 km of seismic reflection data to map the subglacial unconformity that was eroded when WAIS was grounded at the shelf edge, i.e., prior to the deposition of the backstepping GZWs. With respect to the underlying subglacial topography, the first three groundings were slightly basinward of relatively low-relief knolls in the central part of the basin. The remaining four groundings were positioned above the crest of a low-elevation saddle in the center of the WDB. These latter groundings are also located at a significant convergence in the trend of the banks that bound the basin. These observations in the WDB support the general hypotheses that the locations of post-LGM groundings were at least partly controlled by antecedent topography. The results suggest that models seeking to predict ice-sheet response to climate changes should incorporate a highly detailed map of subglacial topography as an important boundary condition.

INTRODUCTION

During the LGM, grounded ice advanced to the Antarctica outer continental shelf and large ice streams, zones of fast flowing ice, eroded wide trough basin that in some cases extended to the continental shelf edge (Fig. 1a). The marine-based WAIS has subsequently retreated hundreds of kilometers to its current position on the inner continental shelf (Conway et al., 1999; Anderson et al., 2014). Pauses in the retreat are recorded by a succession of GZWs that partly fill the trough basins that were eroded during the LGM. Individual GZWs are asymmetrical wedges of sediment deposited at the grounding zone of marine ice streams (Alley et al., 1989). The grounding zone refers to the basinward limit of grounded ice in the marine setting. Sediment flux that constructs the GZWs is delivered by deforming till below the ice stream. In other words, GZWs are essentially subaqueous terminal moraines. The existence of these landforms indicates that the WAIS grounding position was stationary for time intervals that were of duration sufficient to construct large-scale (i.e., seismically-resolvable) GZWs.

Ice sheet reconstructions show that large GZWs are found on the middle continental shelf at similar distances from the continental shelf edge in at least five of the six paleo-ice-stream basins of Ross Sea (Anderson et al., 2014). This distribution of GZWs suggests that the timing and magnitudes of grounding shifts may have occurred in a lockstep fashion and been controlled by a global-scale external control such as post-LGM sea-level rise (Denton et al., 2010). However, the available age controls suggest that the middle shelf GZWs on the Ross Sea continental shelf were not deposited at the same time (Anderson et al. 2014). The middle shelf GZW in the Glomar Challenger Basin in central Ross Sea was deposited slightly prior to the LGM (Bart and Cone, 2012). Conversely, new radiocarbon ages from the WDB in eastern Ross Sea indicate that

grounded ice retreated from the middle continental shelf after the LGM (DeCesare et al., in prep.). This diachroneity between adjacent paleo-ice-streams calls into question a purely eustatic or other pan-Antarctic control on former grounding locations.

Several studies have proposed that subglacial topography is a key factor controlling the grounding line and calving front location during post-LGM retreat (e.g., Jamieson et al., 2012; Batchelor and Dowdeswell, 2015; Matsuoka et al., 2015). The hypothesis is primarily based on the modern seafloor topography as opposed to mapping of the underlying subglacial topography that existed prior to the post-LGM groundings. The objective of this study was to map the unconformity that underlies a post-LGM GZW as a first-order test on the hypothesis that antecedent topography controlled the grounding positions. Because the former grounding line positions are well constrained (Bart et al., 2017a,b) and there is abundant seismic data that can be used to map the unconformity that underlies these deposits, we were able to map the unconformity underlying a GZW cluster in the WDB, a paleo-ice stream trough in eastern Ross Sea (Fig. 1b).

BACKGROUND

WDB bathymetry

The WDB is a paleo-ice stream trough of the WAIS in eastern Ross Sea (Fig. 1b). At the peak of the LGM, the Bindschadler Ice Stream (BIS) occupied the basin (Fig. 1a). The Hayes and Houtz Banks now bound the trough. The cross-trough width averages ~100 km and the trough extends at least ~250 km from the shelf edge southward to where it projects below the Ross Ice Shelf (RIS). The average water depth of the outer and middle continental shelf is ~ 600 meters except at a mid-shelf bathymetric saddle that rises to ~550 meters. The saddle separates the outer and middle continental shelf (Fig. 1b). The bathymetry of the inner continental shelf (below the Ross Ice Shelf) is not well resolved (Bentley and Jezek, 1983).

The mid-shelf bathymetric saddle corresponds to an overlapping stack of seven GZWs in the WDB (Bart et al., 2017a). Bart et al. (2017a) mapped the seafloor geomorphic features from seismic data (Fig. 2) and high-resolution multibeam bathymetry (Supplemental Figure 1). In particular, the boundary between the GZW topset and foreset marks the basinward limit to which the ice stream was grounded prior to retreat to a new grounding position (shown as down-facing arrows on Figure 2). The large volume of the stacked GZWs in the WDB indicates that the grounding line of the paleo-BIS was relatively stationary for >3000 years (Bart et al., 2017b, DeCesare et al., in prep). An isopach map of composite grounding zone wedge (CGZW) shows that these strata are confined to the central part of the basin (Supplemental Figure 2). The seven GZWs all have grounding lines that were within ~75 km of the continental shelf edge. These locations represent a small (~5%) reduction from the LGM extent of grounded ice. Four of the wedges (GZW1, 2, 3, and 7, see Fig. 2) are exposed over large areas of the outer continental shelf. The individual GZWs

cannot be mapped because their bounding surfaces are not regional seismic reflections. Multibeam bathymetric data show that GZW1, 2 and 3 can be traced from the central part of the WDB to the flanks of Hayes and Houtz Banks (Supplemental Fig. 1). This indicates that the grounding line was embayed, i.e., ice was grounded to the shelf edge on the crest of the Hayes and Houtz Bank as it experienced backstepping retreat in the axis of the WDB. Most of the bathymetric saddle and the middle continental shelf correspond to the top of GZW7 (Fig. 2). After the deposition of the middle shelf GZW cluster, the grounding line shifted an additional 200 km south (Bart et al., 2017b; McGlannan et al., 2017). High-resolution chirp transects and multibeam data show that only small-scale morainal ridges mantle the top of the GZW7 topset on the middle continental shelf (Bart et al., 2017a).

Regional seismic stratigraphy of the WDB GZWs

Line 1502B-3 (Fig. 2) is a regional dip-oriented seismic line in TWTT along the central axis of the WDB that extends from the continental shelf edge to the RIS calving front. The transect shows the seven GZWs identified by Bart et al. (2017a, b) and is representative of the key stratal relationships. The GZWs overlie a regional seismic reflector that represents a subglacially-eroded unconformity that formed when the paleo-BIS was grounded at the continental shelf edge during the LGM. Hereafter, we refer to this sub-GZW Unconformity as the Brown Unconformity following Bart (2004). The backstepping GZWs represent a time-transgressive retreat of the BIS. The Brown Unconformity is deeply buried below the stacked GZWs at the middle shelf bathymetric saddle but the unconformity is essentially exposed at the seafloor on the outer continental shelf (below a thin post-LGM layer of glacial marine sediment) (McGlannan et al., 2017).

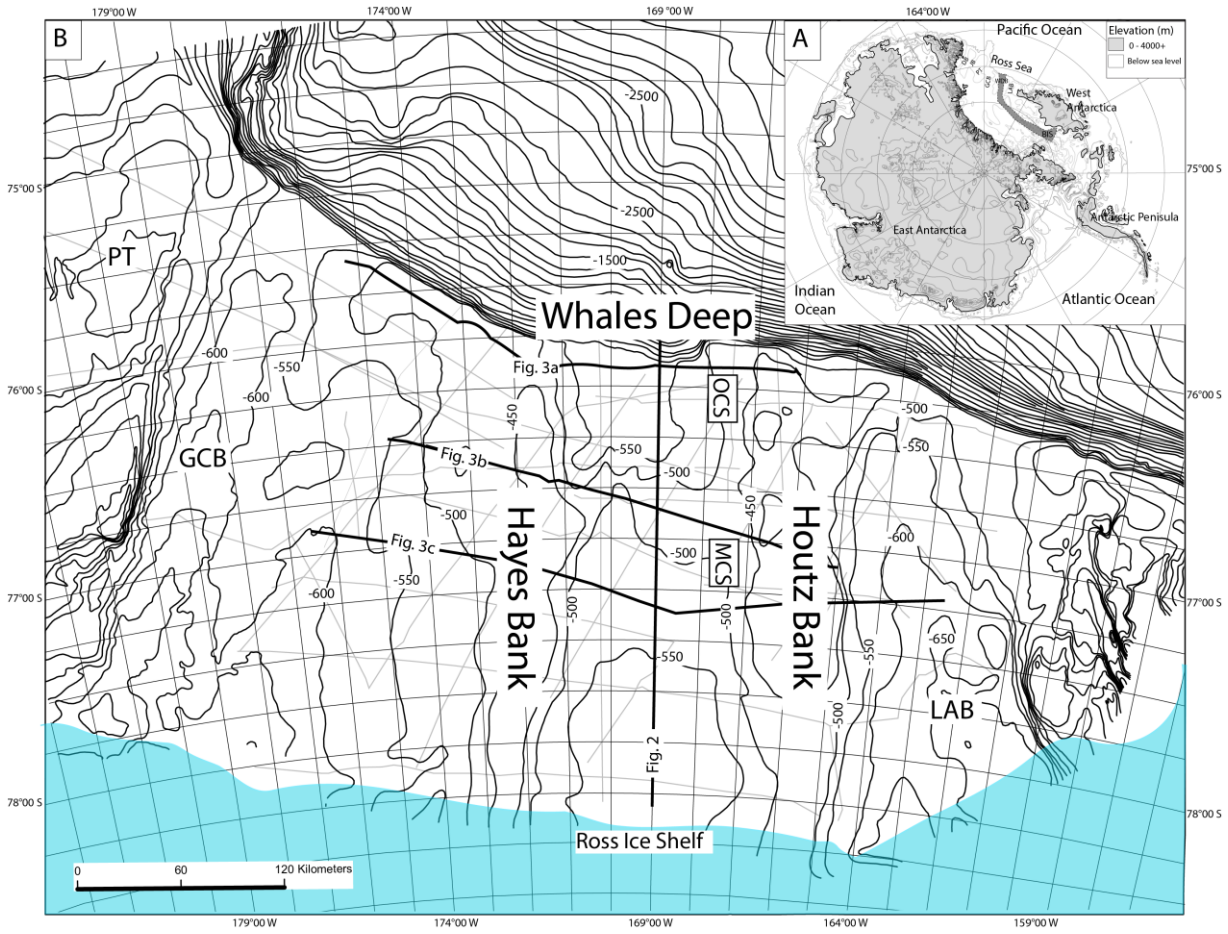

Figure 1: 1a: Ross Sea in relation to Antarctica. The dashed area shows the approximate paleo drainage area of the Bindschadler Ice Stream (BIS) that previously occupied WDB and the paleo-ice stream basins of Ross Sea.
1b: Bathymetric map of Eastern Ross Sea showing WDB as bounded by Hayes and Houtz Banks. The bathymetric saddle on the middle-shelf is comprised of seven GZWs that were deposited since the LGM. The bold black lines indicate the regional seismic cross section shown in Figure 2 and the regional seismically-extracted cross sections in Figure 3 while the thing grey lines indicate the full extent of the seismic grid. Bathymetric contours in meters are from Davey and Nitsche (2013). OCS indicates the outer continental shelf while MCS indicates the middle continental shelf where the bathymetric saddle is located. The ICS is not shown because it is covered by the RIS. Neighboring paleo-ice stream troughs are labeled as such: DB = Drygalski Basin, JB = Joides Basin, PT = Pennell Trough, GCB = Glomar Challenger Basin, LAB = Little America Basin.

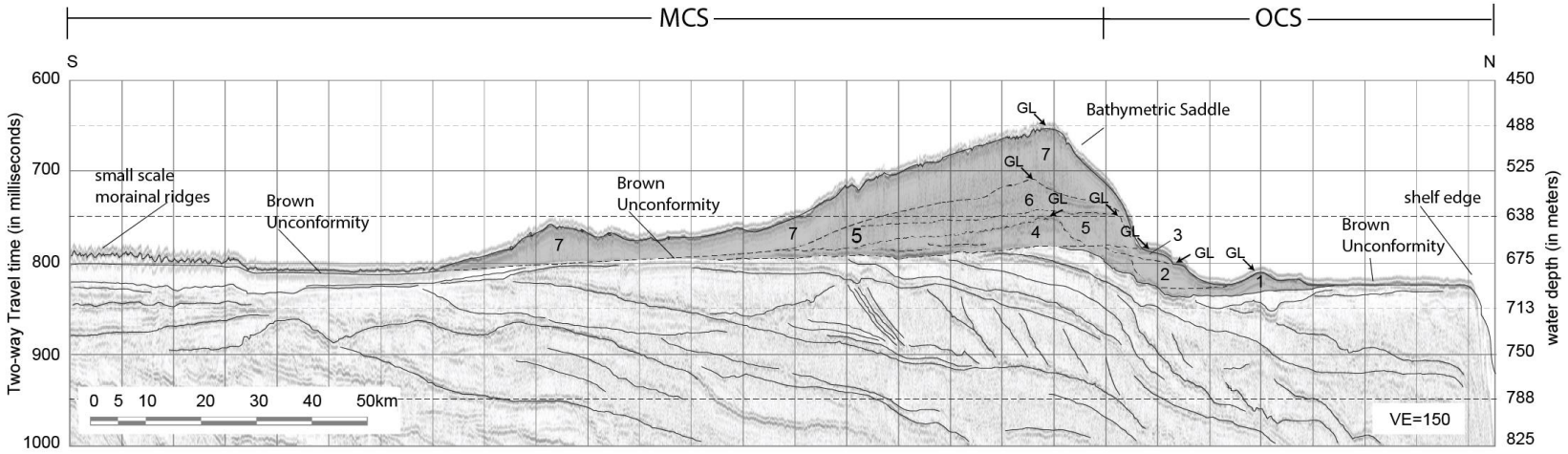

Figure 2: Dip-oriented seismic profile 1502-03 through the axis of Whales Deep trough as indicated by the corresponding line in Figure 1. The 7 grounding lines of the amalgamated GZW cluster are shown. The grounding line of the ice sheet back-stepped to build up the GZW cluster during the post-LGM. OCS indicates the outer continental shelf while MCS indicates the middle continental shelf where the bathymetric saddle is located. The surface beneath the Whales Deep GZW cluster was mapped using seismic data (Adapted from Bart et al., 2017b).

On the outer continental shelf, the unconformity dips slightly towards the south below GZW1 and -2 (Fig. 2). At approximately 50 km from the shelf edge, the dip gradient reverses and the unconformity rises to a broad bench that underlies the thick overlapping stack of GZW4 through -7 at the bathymetric saddle.

At the middle shelf bathymetric saddle, the Brown Unconformity is deeply buried below the stacked GZWs that have a maximum time thickness of 150 msec TWTT. The GZWs gradually thin towards the south but the thinning is more abrupt on the basinward side of the bathymetric saddle. The Brown Unconformity shows clear evidence of truncation of the underlying strata (Fig. 2). On the seismic line, a broad bench on the Brown Unconformity is elevated about 40 msec TWTT above the grade of the surface below the GZWs.

Between the Hayes and Houtz Bank, the thickness and extent of the GZW strata depends on location (Fig. 3a-c). Seismic transects from the outer continental shelf (Fig. 3a) are north of the seismically-resolvable part of the GZWs. The post-LGM sediment has a maximum thickness of 2.5 meters in piston and kasten cores (McGlannan et al., 2017) and this sediment thickness is within the bubble pulse of the seafloor reflection. The Brown Unconformity is essentially equivalent to the seafloor reflection at this transect. The second transect (Fig. 3b) crosses the trough where the stacked GZWs are thickest near the crest of the bathymetric saddle. The third transect crossing the basin on the inner part of the middle continental shelf, shows that the GZWs thin considerably south of the bathymetric saddle (Fig. 3c).

The crest of the bathymetric saddle is roughly aligned with the basinward edge of the subsurface bench of the Brown Unconformity (Fig. 2). South of the bathymetric saddle, the seafloor is foredeepened. Only a cluster of small morainal ridges mantle the top of the GZW7 topset on the

southern end of the line and these have a maximum thickness of 20 msec measured in TWTT (Bart et al., 2017a).

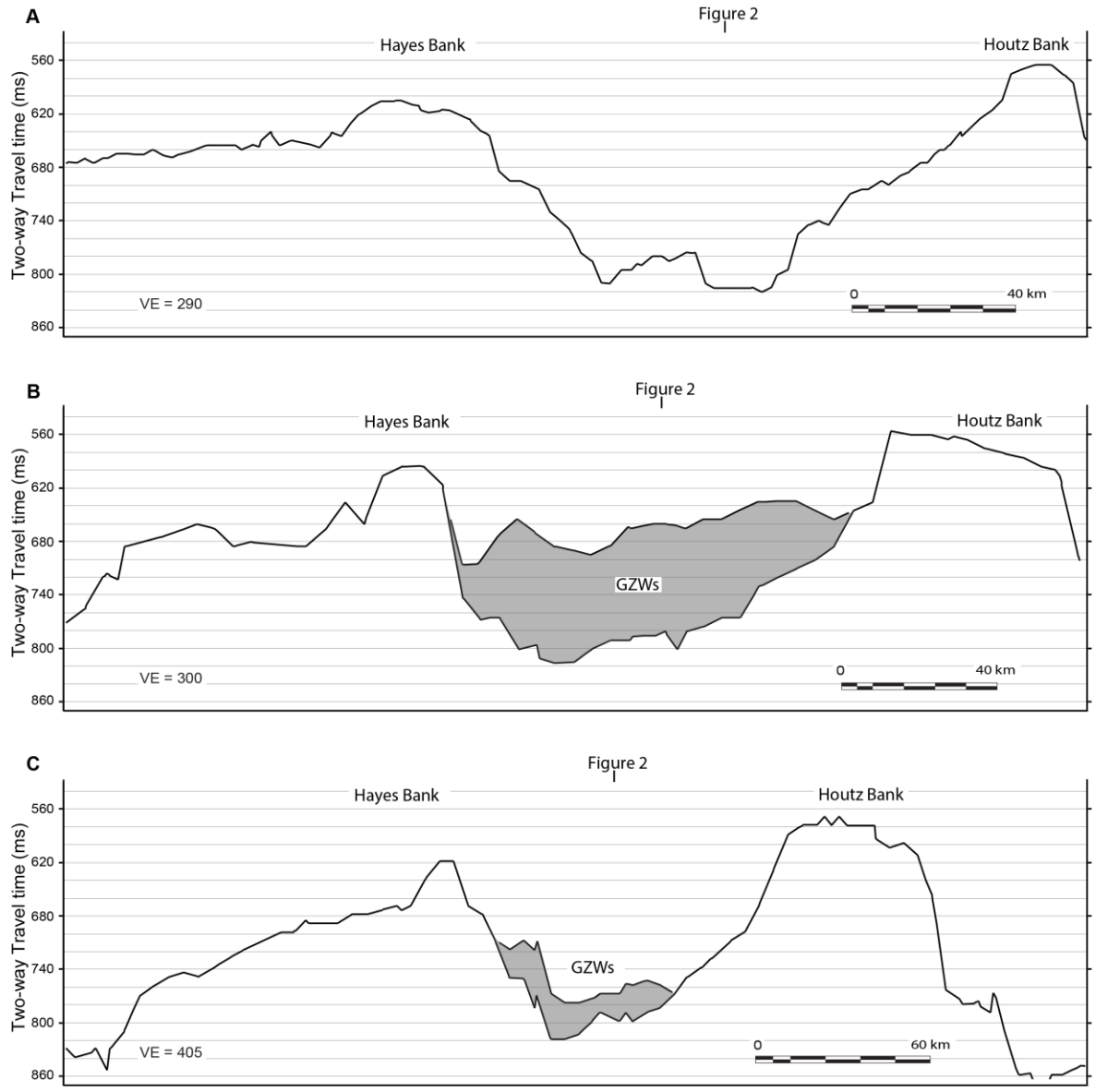

Figure 3: Three seismically-extracted cross sections in the WDB as indicated on the base map. The cross sections are indicated by the corresponding lines in Figure 1. The location of the Figure 2 crossline is also posted.

METHODS

Six seismic surveys were used to map the unconformity that underlies the GZW cluster in the WDB. The surveys were acquired during the following expeditions: PD90, NBP9307, NBP9401, NBP9501, NBP0803, and NBP1502B (Fig. 1). The first five grids are single-channel data acquired using a 50 or 100 cubic inch air gun and single-channel streamer. Shot intervals were every 6 seconds. Underway speed averaged 5 knots. The 2015 grid is multichannel seismic data acquired with a 75 m streamer that generated a maximum fold of 12. The cross lines and timescales were converted to a common scale based on the most recent and highest resolution survey (NBP2015B) to ensure proper correlation of seismic lines acquired in the different surveys. A subset of lines was selected to correlate the subsurface elevation changes of WDB trough and its banks. In total, 38 seismic lines comprising approximately 7500 kilometers of data were used. Two-way travel times (TWTTs) were recorded for the seafloor and Brown Unconformity at a horizontal spacing that ranged from 3 to 4 km. The seafloor reflection TWTTs were converted to depth using a water column velocity of 1500 m/s. The Brown Unconformity corresponds to the seafloor reflection on the crest of Hayes and Houtz Banks (i.e., where the post-LGM GZWs are absent, see Supplemental figure 2). In those places where the Brown Unconformity is overlain by the backstepping GZW strata, the TWTTs for the Brown Unconformity were depth converted using a velocity of 1750 m/s for the overlying GZW based on information presented in Cochrane et al. (1995).

Triangulated irregular networks (TINs) were created for the depth-converted seafloor and the Brown Unconformity using ArcGIS software. The TIN is a 3-D structure created from a non-smoothing interpolation algorithm called Delaunay triangulation. Cross sections were extracted

from the TIN maps to depict the change in the Brown Unconformity and the seafloor. In addition to the computer-generated map, a hand-contoured and smoothed map was created from the same depth-converted data points. The depth-converted Brown-Unconformity contour map was compared to locations of post-LGM WDB grounding lines taken from a high-resolution multibeam bathymetry survey (Bart et al., 2017a).

RESULTS

Depth converted map of the Brown Unconformity

With respect to our objective, the most relevant topographic features are labeled A-J (in Fig. 4). The topography that bounds the WDB (i.e., the shelf edge and the banks) are essentially unchanged relative to their expression in the modern bathymetry (Figs. 1 and 4). Strike and dip-oriented cross sections were extracted from the map to provide additional views of the subsurface features (Figs. 5 and 6). In map view, Hayes Bank is slightly convex towards the WDB (Fig. 4). Above 480 m, the crest of Houtz Bank is significantly wider than Hayes Bank. Houtz Bank rises to ~410 m across a large area of the outer and middle shelf and is about 50 m shallower than Hayes Bank. On the outermost shelf, a large area of Houtz Bank rises above 420 m. In a landward direction, the crest of Houtz Bank exhibits 100 m of foredeepening, i.e., landward dip. In contrast, the narrower crest of Hayes Bank ranges in depth between 450 and 470 m below sea level with three shallower areas: 1) on the outermost shelf; 2) two knolls ~50 km from the shelf edge (i.e., adjacent to the bathymetric saddle); and 3) an elevated region on the inner-part of the middle continental shelf (Fig. 4). The flanks of Hayes and Houtz Banks that face the WDB exhibit variable topography along their lengths. The east flank of Hayes Bank is about twice as steep as the west flank of Houtz Bank (Fig. 4). The steepest grade of Hayes Bank is adjacent to where the trend of the crest is convex towards to the basin. The west flank of Houtz Bank has shallow and uniform dip along its length. Its steepest grade is near the crest between 500 and 420 m at a location that corresponds to the area adjacent to the crest of the bathymetric saddle (Fig. 4).

There are two bank-attached terraces (roughly bound by the 600-m contour) on the east flank of Hayes Bank. The first terrace is on the outermost continental shelf (feature A on Fig. 4).

The second terrace is located on the innermost part of the middle continental shelf (feature B on Fig. 4). Both terraces extend ~50 km towards the center of the basin. The outer-continental shelf terrace (feature A on Fig. 4) has a low-relief knoll at the shelf edge in the center of the trough that rises to approximately 570 m (feature C on Fig. 4). This knoll (feature C) rises 20 m above the rest of the terrace and is 10 km wide in cross section.

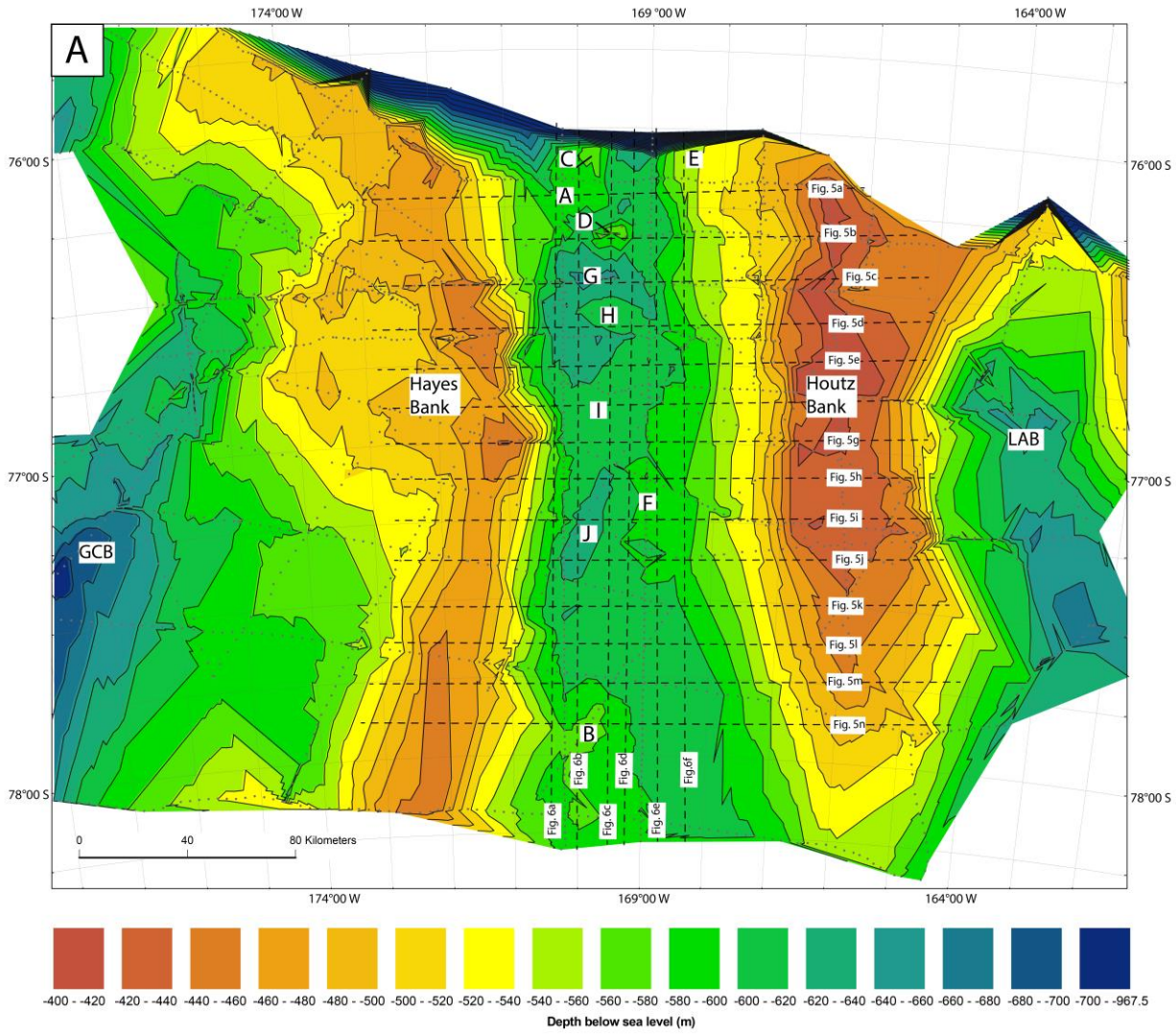

Figure 4A: The depth-converted Brown Unconformity TIN created from the seismic profiles shown in Figure 1 displayed using color. The letters A-J indicate topographic features discussed in the results. The cross section lines indicate transects in Figures 5 and 6.

The terrace and its knoll can be seen in strike and dip transects (Figs. 5a and 6a, respectively). To the south, there is a second knoll isolated from the terrace (feature D on Fig. 4). This feature has similar dimensions to the knoll at the continental shelf edge (35 m height and 10 km width) (Figs. 5b and 6c). On the outermost continental shelf, there is also a small terrace connected to the lower west flank of Houtz Bank (feature E on Fig. 4). In strike and dip views, feature E is a low-angle, basinward dipping terrace on the lower flank of Houtz Bank (Fig. 5a and 6f).

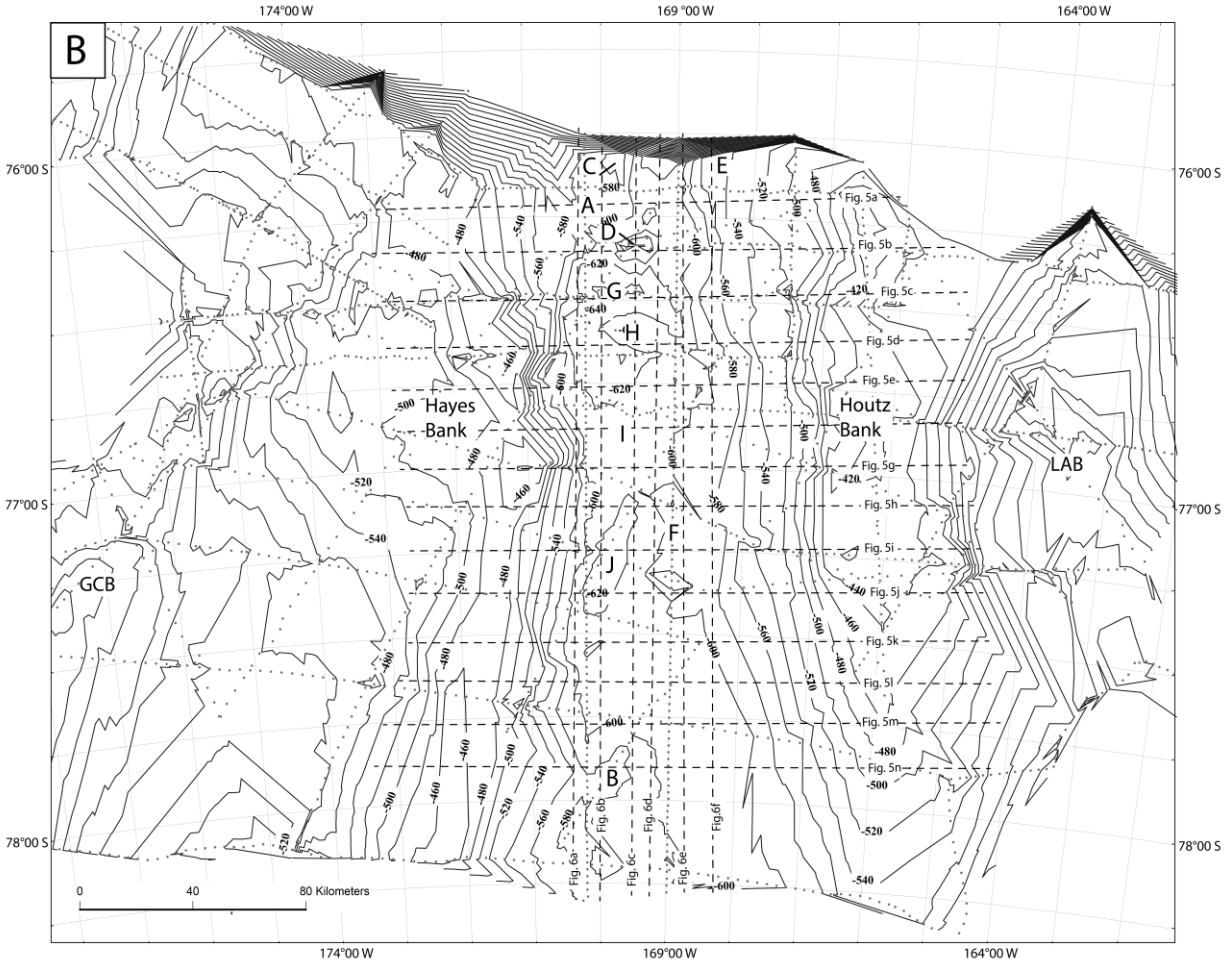

Figure 4B: The depth-converted Brown Unconformity TIN created from the seismic profiles shown in Figure 1 displayed using labeled contours. The letters A-J indicate topographic features discussed in the results. The cross section lines indicate transects in Figures 5 and 6.

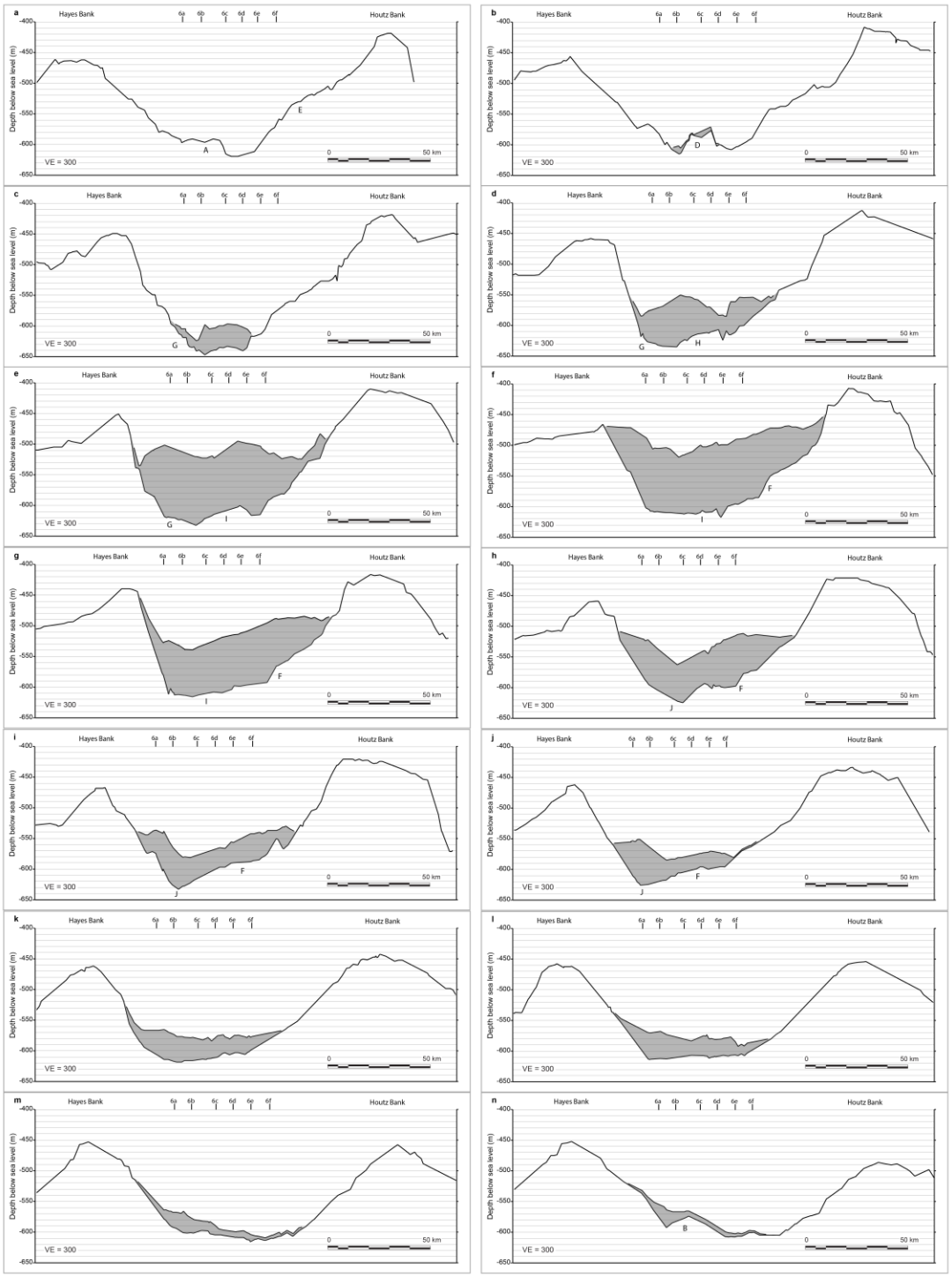

Figure 5: Strike-oriented cross section lines. All of the lines are oriented west to east as indicated on the labeled lines in Figure 4 with A being the farthest north on the outer-shelf and N being the farthest south near the modern calving front. The gray shaded area corresponds to the post-LGM grounding zone wedge cluster. Labeled features A-J are shown on the cross sections as shown on the Brown Unconformity map in Figure 4. The dip crosslines are labeled a-f from Figure 6.

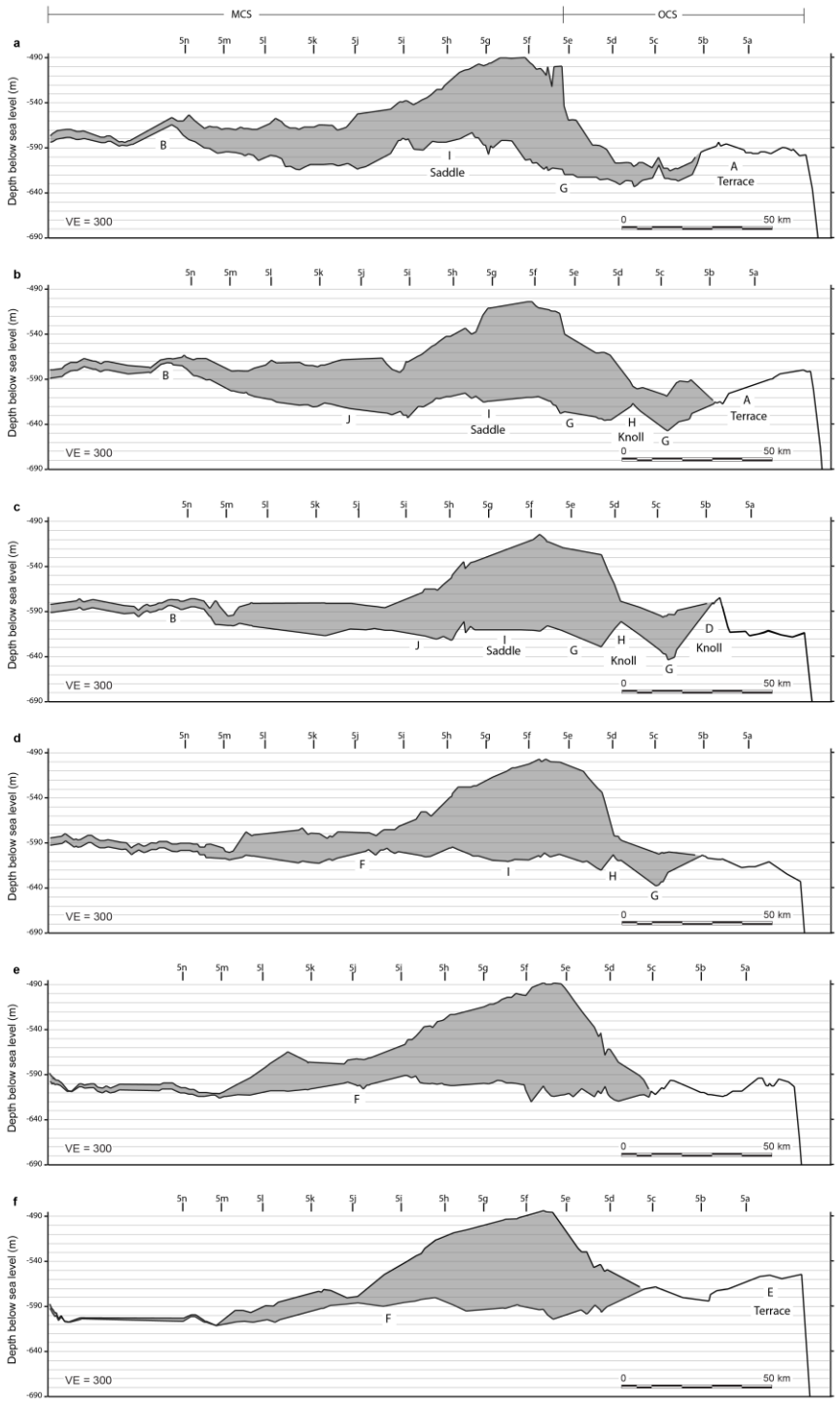

Figure 6: Dip-oriented cross sections. All of the lines are oriented south to north as indicated base map by the labeled lines in Figure 4 with a being the farthest west near Hayes Bank and f being the farthest east near Houtz Bank . The gray shaded area corresponds to the post-LGM grounding zone wedge cluster. Labeled features A-J are shown on the cross sections as shown on the Brown Unconformity map in Figure 4. The strike crosslines are labeled a-n from Figure 5.

On the inner part of the middle shelf, an irregularly shaped elevated area rises above the low-grade of the terrace of the Hayes Bank (feature B on Fig. 4). Elsewhere, the eastern flank of Hayes Bank reaches the basin floor roughly parallel with the crest of Hayes Bank at the 600-m contour. A broad terrace is also seen on the western flank of Houtz Bank at a distance of 85-150 km from the shelf edge (feature F on Fig. 4). The terrace (feature F) extends approximately 20 km into the central part of the WDB (Fig. 5i).

The central part of the WDB has depths that range from 600-640 m. Most of the basin has only slight relief ranging between 600-620 meters depth. Between these depth ranges, the basin exhibits slight sinuosity relative to the more linear north-south orientation of the Hayes and Houtz Banks. The basin bends around the terraces on the lower bank flanks (Fig. 4).

The trend of the shelf edge is indented by two re-entrants. To the south, the deepest parts of the WDB include two irregularly-shaped depressions. At ~40 km from the shelf edge, just to the south of the isolated knoll (feature D on Fig. 4), there is a 50 m wide irregular area with depths ranging from 600 to 640 m. The deepest area (below 620 m) has an arcuate “c”-shape in map view, immediately south of the isolated knoll (feature G on Fig. 4). The north part of the c-shape deepens to 640 m in a roughly east-west zone 25 km wide area. To the south of this depression, the topography rises to a broad east-west oriented feature connected to Houtz Bank (feature H on Fig. 4). This feature rises to 610 m and extends more than half-way across the basin. This feature can also been seen in dip cross sections as a small bump on the outer-shelf bounded to the south and north by trenches (Figs. 5d and 6 b-d). To the south of this elevated area, the basin deepens to more than 620 meters. The central part of the basin is a low-relief saddle defined by the 620 m contour (feature I on Fig. 4). In cross section view, this saddle is seen as a broad bench

(Figs. 5e and 6a). The southern-side of the saddle is partly defined by the west-facing terrace of Houtz Bank (feature F on Fig. 4). Immediately to the west of the Houtz Bank terrace, the west side of the WDB deepens to 630 m in a 50-km long elongated depression (feature J on Fig. 4). South of this depression, the basin as defined by the 600 m contour shallows and bends around the terrace on the eastern side of Hayes Bank (feature B on Fig. 4) on the middle continental shelf.

Hayes-Houtz bottleneck

The width of the paleo-ice stream trough basin was measured at the 500 m contour. From the shelf edge, east-west cross sections (Fig. 5) show that the distance between the banks narrows at the location where the GZWs stack and then widens towards the RIS calving front. On the outermost shelf, the trough width ranges from 110-120 km (Figs. 5a, b). The middle shelf cross sections (Figs. 5e-i) traverse the region of the middle shelf bathymetric saddle and the thickest accumulation post-GZW strata in WDB. Here, the width constricts to between 85 and 95 km (below the bathymetric saddle at GZW7) (Figs. 5h, g), which is greater than a 25 % reduction from the maximum observed trough width on the outer shelf (Fig. 5b). The trough width widens to 125 km on the innermost part of the middle shelf (Fig. 5n) which is a 45% widening of the banks.

Post-LGM grounding line positions superimposed on the Brown Unconformity topography

The location of the former grounding line positions that were mapped from the seismic and multibeam survey (Fig. 2 and Supplemental Figure 1) are shown as lines super-imposed on the Brown Unconformity topography (Fig. 7). The LGM grounding was at the continental shelf edge, which constitutes the maximum possible extent of grounded ice. The overlay shows that

the embayment trend of GZW1 grounding line is aligned with the two outer-shelf knoll features in the west (features C and D on Fig. 7). On the eastern side of the basin, the GZW1 grounding line was located on the basinward-dipping flank of Houtz Bank where it slightly protrudes towards the center of the basin (feature E on Fig. 7).

GZWs 2 and 3 are exposed over a large area in the center of the basin. Here, the GZW2 and 3 grounding lines are positioned above a basinward-dipping surface that rises to the east-west oriented knoll that is partly attached to Houtz Bank (feature H on Fig. 4). The location of the GZW3 grounding line in particular corresponds with knoll that is surrounded by the c-shaped depression (feature H on Fig. 4). The GZW2 and 3 grounding lines are perched on the basinward-dipping lower flank of the Houtz Bank (feature E on Fig. 4). Only the GZW 2 grounding line is exposed on the western side of the basin. Here, its backstep location is positioned on the basinward-dipping lower flank of the Hayes Bank. The grounding line for GZWs 4 through 7 are generally aggradational and are slightly basinward of the broad middle shelf saddle (feature I on Fig. 4). The grounding lines for these four GZWs roughly correspond to the location where the width of the trough narrows.

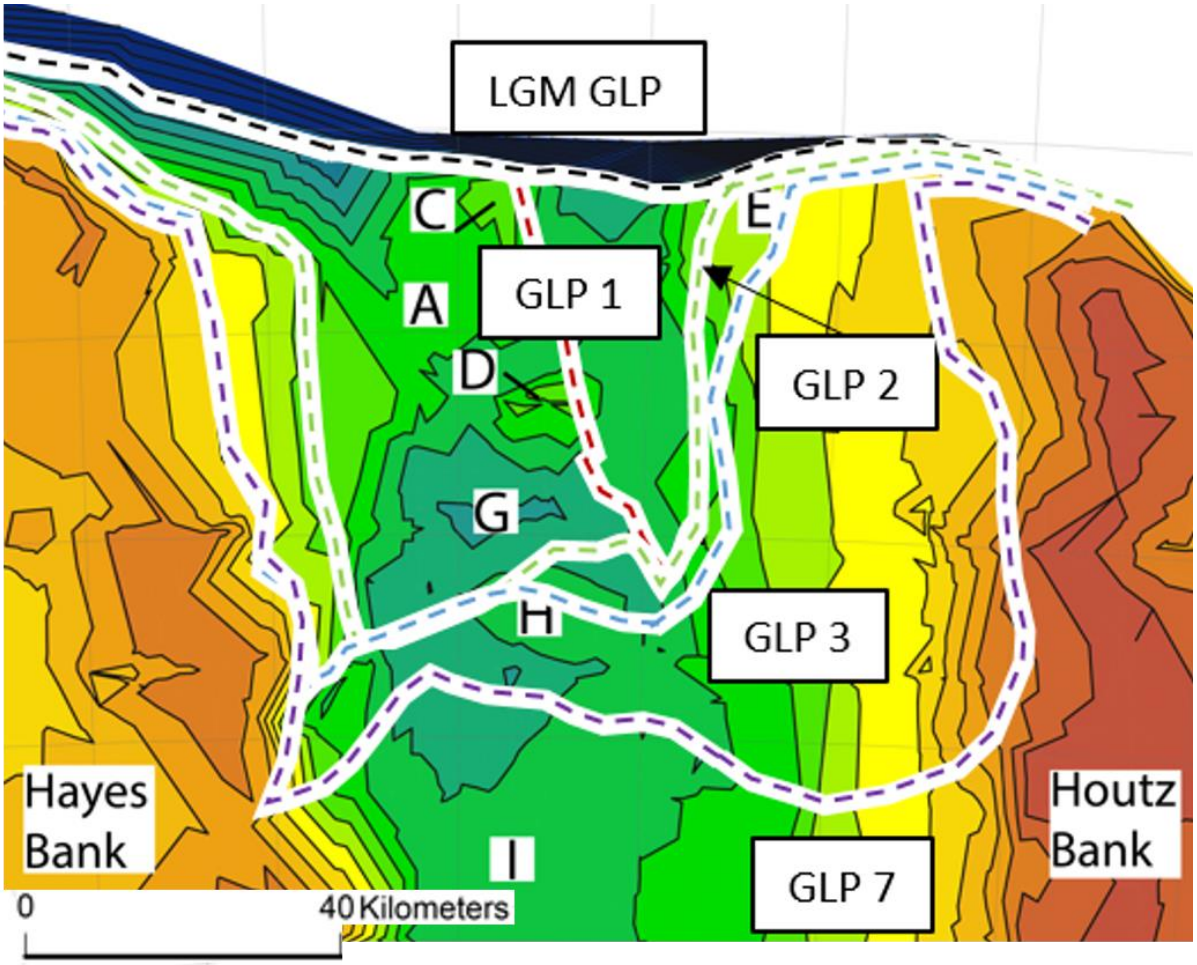

Figure 7: The depth-converted map with labeled topographic features is shown with a focus on the outer and middle shelf where the post-LGM groundings occurred. The post-LGM grounding lines mapped from high-resolution multi-beam bathymetry shown in Supplemental Figure 1 are also placed on this map to show the different locations the WAIS grounded during the deposition of the post-LGM GZW cluster on this reconstruction of the Brown Unconformity. These grounding line positions (GLPs) are labeled LGM, 1, 2, 3, 7 based on the sequence of groundings.

DISCUSSION

The discussion is sub-divided into four parts. Part 1 considers the interpretability of the Brown Unconformity map. Part 2 presents our interpretation of how the WDB grounding line positions were related to antecedent topography of the Brown Unconformity and consider the buoyancy limits for grounded ice. In Part 3, we compare our results to other published examples of how the locations of other post-LGM GZWs relate to topography.

The Brown Unconformity subglacial topography

To evaluate the degree to which the choice of sediment velocity influences the Brown-Unconformity topography, we created a series of time-depth conversions using a range of higher and lower velocities (Fig. 7a-c). In the particular case of the WDB, a subsurface map in TWTT (Supplemental Figure 3) yields a very similar topography as the T-D conversions. A review of these maps show that the choice of time-depth conversions caused only a minimal effect on the reconstruction of the basin topography beneath the post-LGM sediment (Figure 4). The greatest difference between conversions is for the middle shelf areas where the GZW cluster is thickest. However, the differences in reconstructed elevation are small (i.e., a maximum 25 m from slowest to fastest velocity). After deglaciation, formerly ice-covered landscapes rebound to achieve isostatic balance (Parizek and Alley, 2004; Whitehouse and Bradley, 2012). As specifically pertains to the retreat of grounded ice in WDB, there has been only minimal deflation of the ice sheet surface at Siple Dome since the LGM (Waddington et al., 2005). In other words, the paleo-BIS probably had a low surface profile between the continental shelf edge and Siple Coast during the LGM and post-LGM time.

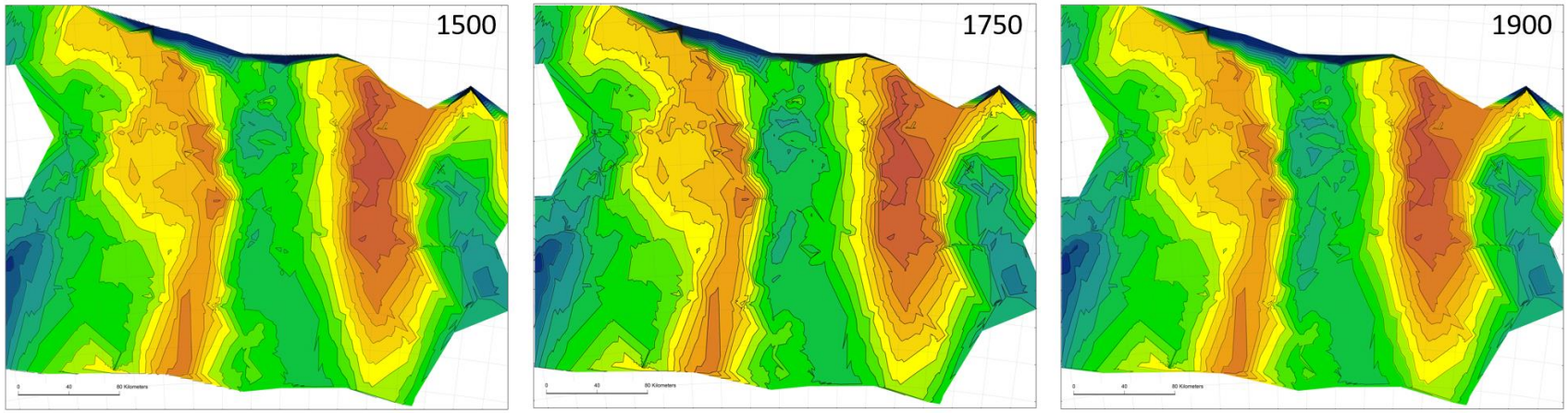

Figure 8: TIN reconstruction maps for the Brown Unconformity. Three velocities were used to determine the sensitivity of the reconstructed bathymetry to depth conversion. While 1750 m/s was used as the velocity for the depth conversion process based on previous work, the maps using the other velocities for the post-LGM sediment are provided to compare the differences.

The modern ice sheet exhibits similar small decrease in surface elevation over the 300 kilometers inland of its marine termination (Fretwell et al., 2013). On these bases, we discount the possibility that a significant differential in post-LGM rebound occurred between the outer and middle continental shelf in the time since grounded ice vacated the WDB trough.

Subglacial erosion and topography relief

Larger-scale trough bank topography is clearly evident on the Brown Unconformity (Fig. 4). Variations in the elevation of the trough basin are also present but micro-scale glacial features such as mega-scale glacial lineations, drumlins, and craig and tail features with dimensions less than a few meters (Glasser and Bennett, 2004) are too small to map with a seismic grid of this density and resolution. The smallest resolved features in the basin include knolls, saddles and depressions (Fig 4). In formerly ice-covered areas, these features are eroded by subglacial abrasions and quarrying (Hindmarsh, 1996). The mapped topographic relief is relatively low and probably reflects small variations in erodible substrates. The ages of the strata underlying the Brown Unconformity young in the direction of the shelf edge based on their overall basinward tilt. Correlation to DSDP Leg 28 sites in eastern Ross Sea (Hayes and Frakes, 1973) indicate that the strata underlying the Brown Unconformity range in age from Miocene to Pleistocene. The lithification of these strata ranged from consolidated at Sites 270 to mostly unconsolidated at Sites 271 and 272.

The low-relief Brown-Unconformity saddle near the boundary between the outer and middle continental shelf is slightly landward of the modern seafloor bathymetric saddle (feature I on Fig. 4). Its gentle asymmetric form suggests gradual erosion by abrasion on its southern side and quarrying on its more steeply-dipping basinward side (Hindmarsh, 1996; Glasser and

Bennett, 2004). The saddle is significantly larger than whalesbacks (Evans, 1996) but is nonetheless clearly a subglacially-eroded feature. Based on its dimensions, the subsurface saddle at the Brown Unconformity is equivalent to a large-scale roche moutonnee as described by Gordon (1981).

Basinward of this saddle, the depression on the outer continental shelf (feature G on Fig. 4) corresponds to a zone of enhanced erosional quarrying. The scour is located basinward of the subsurface saddle in an area where the trend of the Hayes and Houtz Banks diverge. When the paleo-BIS was grounded at the shelf edge, ice-stream flow past this constriction (in both the trough width and depth, see Fig. 4) would have been associated with a decrease in pressure. The less-confined ice-stream flow on the outer continental shelf may have been associated with the freezing of basal meltwater, which would have aided erosional quarrying and plucking of material (Hallet, 1996) to create this erosional depression during the LGM when the paleo-BIS was grounded at the continental shelf edge.

WDB groundings at low-relief outer-shelf knolls and the middle-shelf saddle

If topography was an important control on grounding position, then the former grounding lines should be in relatively Hays close proximity to antecedent topography of the Brown Unconformity. Below we review how the mapping results provide the first demonstration that a correlation exists between grounding location and antecedent topography in the form of low-relief features and trough width.

The subsurface relief of the Brown Unconformity is relatively low. The clustering of grounding lines on low-relief features on the outer continental shelf is generally consistent with the observation that the Brown-Unconformity does not exhibit any significant foredeepening

(which otherwise is associated with rapid, large-distance grounding-line retreat as shown by Bamber (2009)).

The WAIS attained its maximum extent at the LGM as indicated by mega-scale glacial lineations that extend to the shelf edge (Mosola and Anderson, 2006; Bart et al., 2017b). The continental shelf width was an ultimate topographic control on the extent of grounded ice during the LGM. Upon retreating from its shelf-edge position, the grounding line first became embayed on the eastern side of the outer continental shelf basin but remained grounded at the shelf edge on the western side of the trough at the GZW1 GLP (Fig. 7). This embayment is consistent with the view that lift-off of marine-based ice from the seafloor partly depends on water depth (Le Meur et al., 2014; Matsuoka et al., 2015; Bart et al., 2016). Ice apparently remained grounded on the basinward-sloping flanks of the Hayes and Houtz Bank (Figs. 5a, e) (Bart et al., 2017a; McGlannan et al., 2017). Similar grounding-line embayments of backstepping grounding zone features are found on the flanks of western Ross Sea banks (Shipp et al. 1999; Halberstadt et al., 2016).

In the center of the basin, the trend of the WDB embayment during the GZW1 grounding strongly suggests that ice was at least temporarily pinned at the two low-relief knolls on the outer continental shelf (features C and D on Fig. 7). A modeling study of the Foundation Ice Stream showed that a vertical pinning point directly landward of the grounding position permitted the ice sheet to stably maintain a grounding position even in a deep trench (Huybers et al., 2017). The modern WAIS grounding lines have similar larger-scale embayments (Ross et al., 2012) but the bathymetry below the large RIS is too poorly resolved (Jezek and Bentley, 1983; Fretwell et

al., 2013) to determine if similar knolls or other low-relief structures are associated with these modern grounding locations.

The grounding lines of GZW2 and -3 shifted south over the erosional depression on the outer continental shelf before re-grounding on the shoaling flank of the small knoll that is attached to lower flank of the Houtz Bank (Fig. 7). These two grounding positions on the basinward dipping flank of a knoll is consistent with predictions of modeling studies of retreating marine-based ice sheets which show grounding lines migrating rapidly over foredeepened seafloors and decelerating on basinward-dipping seafloors (Joughin et al., 2002). The presence of sub-ice-shelf sediments overlying the foresets of GZW1, -2 and -3 diamicts on the outer continental shelf (McGlannan et al., 2017) strongly suggests that these grounding lines remained pinned on the basinward-dipping flank of Hayes and Houtz Bank.

Given the progressive aggradation of sediment represented by the overlapping stack of GZW4 through -7, the buried antecedent topography on the Brown Unconformity would have through time been able to exert less influence on grounding location. The locations of the GZW4 through -7 groundings lines are slightly basinward of the Brown-Unconformity saddle as well as a significant narrowing of the trough width (Fig. 7). Jamieson et al. (2012) inferred grounding lines stabilize as the ice-stream retreats through bank-bank constrictions. The narrowing of the ice-stream cross section would have slowed and stabilized ice-stream discharge (Joughin et al., 2002). An increase in lateral drag from the narrowing of the trough width reduces ice flow velocities and provides stability by decreasing the flux of ice across the grounding zone (Echelmeyer et al., 1991; Whillans and Van der Veen, 1997; Joughin et al., 2004). The trough-width bottleneck provides strong evidence that topography influenced grounding. Modeling

studies predict that an ice sheet could stabilize even on a foredeepened seafloor if the trough narrows (Docquier et al., 2014).

The available age control indicates that grounding at this time was maintained until 11.5 cal kyr BP. The aggradational stacking (of GZW4 through -7) progressively steepened the subglacial profile. This newly formed foredeepened topography associated with GZW sediment aggradation is a substantial modification to the near-horizontal dip of the underlying Brown Unconformity. Hence, the aggradational stack of GZWs created the foredeepened topographic criteria that triggered abrupt, large-distance retreat of grounded ice that is described by the marine-ice-sheet instability hypothesis (Weertman, 1974). Indeed, the long-duration grounding at the bathymetric saddle was followed by an abrupt 200-km grounding line retreat. We infer that stable grounding position (represented by GZW4 through -7), was probably aided by the rapid aggradation of GZW4 through -7 (Anandakrishnan et al., 2007; Alley et al., 2007; McGlannan et al., 2017). Rapid deposition would have been associated with accelerated ice-stream discharge after the loss of the ice shelf buttressing at 12.3 cal. kyr BP (DeCesare et al, in prep.) Loss of ice shelf buttressing is thought to be associated with rapid retreat (Matsuoka et al., 2015). The sedimentation filled accommodation as the ice-stream deflated and sea-level rose.

These former grounding locations in the WDB would have ultimately been controlled by the combination of continental shelf depth and ice-sheet thickness (Bart et al., 2016; Jakobsson et al., 2016). For any given continental shelf depth, there exists a theoretical buoyancy limit for grounded ice (Le Meur et al., 2014). The minimum ice thickness that must exist to maintain the paleo-grounding line, H_g, is estimated using equation (1) from Huybers et al., (2017), where z_g is

the water depth (in meters below paleo sea level) at the grounding line, and p_w and p_i are the densities of seawater and ice (1028 kg/m^3 and 900 kg/m^3, respectively).

$$H_g = z_g*(p_w/p_i) \quad (1)$$

Based on the grounding times (DeCesare et al., in prep.) and the associated post-LGM sea-level rise (Peltier and Fairbanks, 2006), the paleo-BIS would have to had minimum thicknesses (at the grounding line) that ranged from 500-600 m (See Supplemental Table 1) to remain grounded. This range of ice-stream thicknesses is slightly shallower than modern ice streams that are grounded on the overdeepened and foredeepened inner continental shelves (Ross et al., 2012). Irrespective of the extant continental shelf depth, as the grounding line of a marine-based ice sheet retreats over even low-relief protrusions (in the subglacial topography), the grounding line of the retreating ice sheet will tend toward stability if the ice-stream thickness exceeds the buoyancy limit (Le Meur et al., 2014; Huybers et al., 2017). The data from the WDB suggests that the trough bottleneck and even relatively low relief protrusions such as the knolls on the outer continental shelf on the Brown Unconformity were sufficient to cause the grounding line position to stabilize.

Comparison with other post-LGM and modern groundings

Even as more and more GZWs are identified on Antarctic and Arctic margins (e.g., Batchelor and Dowdeswell, 2015), it remains difficult to assess the degree to which post-LGM grounding locations were controlled by antecedent topography because the underlying unconformities are not mapped. Strictly based on published 2D seismic transects and modern bathymetry, several post-LGM groundings appear to be situated over the crest of bathymetric saddles where the trough width narrows. Such a correspondence between GZW location and

topography exists in the Drygalski Trough and Pennell Trough basins in western Ross Sea (Shipp et al., 1999). The Drygalski Trough has a large GZW that formed adjacent to Coulman Island. Matsuoka et al. (2015) noted that the modern grounding lines and calving front are anchored at both subaerial islands and shallow submarine banks. In the Amundsen Sea sector, a backstepping cluster of GZWs on the outer and middle continental shelf of the Pine Island Trough overlies an elevated bench and forms a bathymetric saddle that also corresponds to a location where the trough narrows (Lowe and Anderson, 2002; Graham et al., 2010). The largest wedge of the cluster, GZW5, overlies the crest of the bathymetrically-expressed saddle and is adjacent to a prominent topographic feature, Burke Island. The middle shelf GZW in the Glomar Challenger Basin, the trough immediately west of WDB (Bart and Owolana, 2012) has a similar volume to the WDB GZW cluster. Its subglacial topography is not yet mapped. However, the Glomar Challenger Basin GZW is adjacent to Ross Bank, a large-area shallow submarine bank that rises to less than 180-m depth. Its shallow depth and broad extent must have slowed ice flow in the adjacent trough basins.

The absence of large-scale GZW from broad sectors of trough basins is also significant. Generally speaking, GZWs are absent across broad areas of foredeepened topography of modern inner continental shelves (Shipp et al., 1999; Wellner et al., 2001, Klages et al., 2014; Larter et al., 2014). The occurrence of only small-scale morainal ridges mantling the foredeepened topset of GZW7 is consistent with the view of topographic control on grounding location. In the case of the WDB, the absence of GZWs appears to correspond with foredeepened seafloors and/or an absence of other topographic elements that might have otherwise buttressed ice-stream and ice shelf flow. A fundamental tenet of the Marine Ice Sheet Instability Hypothesis is ice sheets retreat

rapidly across a foredeepened (landward-dipping) surface (Weertman, 1974; Bamber, 2009). In Marguerite Bay, a well-surveyed large paleo-ice-stream trough basin on the western margin of the Antarctic Peninsula, small-scale backstepped GZWs mantle the foredeepened seafloor (Jamieson et al., 2011). These small-scale GZWs suggest that the grounding line experienced relatively continuous and rapid retreat with only short intervals during which the grounding line was stationary in places where topographic features are absent.

CONCLUSION

The reconstructed topography of the Brown Unconformity in the WDB shows that post-LGM grounding locations were in proximity to topographic relief that included low-relief knolls, on the outermost shelf, a broad roche mountonee on the middle shelf and a constriction in the trough width. While there is a positive correlation between WDB grounding line locations and antecedent topography, we cannot eliminate the possibility that other factors also played a significant role. These findings suggest that ice-sheet models should include subglacial topography as an important boundary condition that should be considered.

REFERENCES

Alley, R.B., Blankenship, D.D., Rooney, S.T., Bentley, C.R., 1989, Sedimentation beneath the ice shelves – the view from Ice Stream B: Marine Geology, v. 85, pp 101-120.

Alley, R.B., Anandakrishnan, S., Dupont, T.K., Parizek, B.R., and Pollard, D., 2007, Effects of Sedimentation on Ice-Sheet Grounding-Line Stability: Science, v. 315.

Anandakrishnan, S., Voigt, D.E., Alley, R.B., and King, M.A., 2003, Ice stream D flow speed is strongly modulated by the ti de beneath the Ross Ice Shelf: Geophysical Research Letters, v. 30, p. 1–4, doi: 10.1029/2002GL016329.

Anandakrishnan, S., Catania, G., Alley, R.B., and Horgan, H.J., 2007, Discovery of till deposition at the grounding line of Whillans Ice Stream.: Science, v. 315, p. 1835–1838, doi: 10.1126/science.1138393.

Anderson, J.B., Conway, H., Bart, P.J., Kirshner, A.E., Greenwood, S.L., McKay, R.M., Hall, B.L., Ackert, R.P., Licht, K., Jakobsson, M., and Stone, J.O., 2014, Ross Sea Paleo-Ice Sheet Drainage and Deglacial History During and Since the LGM, Quaternary Science Reviews, http://dx.doi.org/10.1016/j.quascirev.2013.08.020

Bamber, J.L., 2009, Reassessment of the Potential Sea-Level Rise from a Collapse of the West Antarctic Ice Sheet: v. 901, p. 901–904, doi: 10.1126/science.1169335.

Bart, P.J., 2004, West-directed flow of the West Antarctic Ice Sheet across eastern basin, Ross Sea during the Quaternary. Earth and Planetary Science Letters 228, 425-438.

Bart, P.J., Cone, A.N., 2012, Early stall of West Antarctic Ice Sheet advance on the eastern Ross Sea middle shelf followed by retreat at 27,500 14C yr BP. Palaeogeography, Palaeoclimatology, Palaeoecology v. 335-336, p. 52–60, doi:10.1016/j.palaeo.2011.08.007

Bart, P.J., and Owolana, B., 2012, on the duration of West Antarctic Ice Sheet grounding events in Ross Sea during the Quaternary: Quaternary Science Reviews, v. 47, p. 101–115, doi: 10.1016/j.quascirev.2012.04.023.

Bart, P.J., Anderson, J.B., and Nitsche, F.O., 2017a, Post-LGM grounding-line positions of the Bindschadler Ice Stream in Ross Sea: Journal of Geophysical Research: Earth Surface, v. Submitted, doi: 10.1002/2017JF004259.

Bart, P.J., Krogmeier, B.J., Bart. M.P. and Tulaczyk, S.M., 2017b, The paradox of a long grounding during West Antarctic Ice Sheet retreat in Ross Sea: Scientific Reports v. 7, article 1262, doi:10.1038/s41598-017-01329-8.

Batchelor, C.L., Dowdeswell, J.A., and Pietras, J.T., 2014, Evidence for multiple quaternary ice advances and fan development from the Amundsen gulf cross-shelf trough and slope, Canadian Beaufort sea margin: Marine and Petroleum Geology, v. 52, p. 125–143, doi: 10.1016/j.marpetgeo.2013.11.005.

Batchelor, C.L., and Dowdeswell, J. a., 2015, Ice-sheet grounding-zone wedges (GZWs) on high-latitude continental margins: Marine Geology, v. 363, p. 65–92, doi: 10.1016/j.margeo.2015.02.001.

Cochrane, G.R., De Santis, L., Cooper, A.K., 1995. Seismic Velocity expression of glacial sedimentary rocks beneath Ross Sea from sonobuoy seismic-refraction data. In: Cooper, A.K., Barker, P.F., Brancolini, G. (Eds.), Geology and Seismic Stratigraphy of the Antarctic Margin. Antarctic Research Series, vol. 68, pp. 261-270.

Conway, H., Hall, B.L., Denton, G.H., Gades, A.M., and Waddington, E., 1999, Past and future grounding-line retreat of the West Antarctic ice sheet: Science, v. 286, p. 280–283.

Davey, F., (2013). Contours of Ross Sea Bathymetry (2004). Integrated Earth Data Application (IEDA). doi: http://dx.doi.org/10.1594/IEDA/100406.

Davey, F. and Nitsche, F. (2013). Ross Sea bathymetry grid (2005) based on Fred Davey's bathymetry map (2004). Integrated Earth Data Applications (IEDA). doi: http://dx.doi.org/10.1594/IEDA/100405 .

Docquier, D., Pollard, D., and Pattyn, F., 2014, Thwaites Glacier grounding-line retreat: Influence of width and buttressing parameterizations: Journal of Glaciology, v. 60, p. 305–313, doi: 10.3189/2014JoG13J117.

DeCesare, M., Bart, P.J., Majewski, W., McGlannan, A., Rosenheim, B.E., 2017,West Antarctic Ice Sheet retreat in eastern Ross Sea during Meltwater Pulses 1a and 1b: in preparation.

Echelmeyer, K., Clarke, T.S., and Harrison, W.D., 1991, Surficial glaciology of Jakobshavn Isbrae, West Greenland: Part I. Surface Morphology: Journal of Glaciology, v. 37, p. 368–382.

Evans, I.S., 1996, Abraided rock landforms (whalebacks) developed under ice streams in mountain areas, Annals of Glaciology, v. 22, p. 9-16.

Fretwell, P., Pritchard, H.D., Vaughan, D.G., Bamber, J.L., Barrand, N.E., Bell, R., Bianchi, C., Bingham, R.G., Blankenship, D.D., Casassa, G., Catania, G., Callens, D., Conway, H., Cook, A.J., et al., 2013, Bedmap2: Improved ice bed, surface and thickness datasets for Antarctica: Cryosphere, v. 7, p. 375–393, doi: 10.5194/tc-7-375-2013.

Glasser, N.F., and Bennett, M.R., 2004, Glacial erosional landforms: Origins and significance for palaeoglaciology, Progress in Physical Geography, v. 28, p. 43–75, doi: 10.1191/0309133304pp401ra.

Gordon, J., 1981, Glacier Margin Fluctuations during the 19th and 20th Centuries in the Íkamiut Kangerdluarssuat Area, West Greenland, Arctic and Alpine Research, v. 13, p. 47-62, doi:10.2307/1550625.

Graham, A.G.C., Larter, R.D., Gohl, K., Dowdeswell, J.A., Hillenbrand, C.D., Smith, J.A., Evans, J., Kuhn, G., and Deen, T., 2010, Flow and retreat of the Late Quaternary Pine Island-Thwaites palaeo-ice stream, West Antarctica: Journal of Geophysical Research: Earth Surface, v. 115, p. 1–12, doi: 10.1029/2009JF001482.

Halberstadt, A.R.W., Simkins, L.M., Greenwood, S.L., and Anderson, J.B., 2016, Past ice-sheet behavior: retreat scenarios and changing controls in the Ross Sea, Antarctica: The Cryosphere, v. 10, p. 1003–1020, doi: 10.5194/tc-10-1003-2016.

Hallet, B., 1996, Glacial quarrying: A simple theoretical model, Annals of Glaciology, v. 22: p. 1-8.

Hayes, D.E. and Frakes, L.A., 1975, General synthesis, Deep Sea Drilling Project Leg 28. In: D.E. Hayes, L.A. Frakes et al., Initial Reports of the Deep Sea Drilling Project, 28. U.S. Govt. Printing Office, Washington, D.C., p. 919--942.

Hindmarsh, R., 1996, Stochastic perturbation of divide position. Annals of Glaciology, 23, p. 94-104, doi: 10.3189/S0260305500013306.

Huybers, K., Roe, G., and Conway, H., 2017, Basal topographic controls on the stability of the West Antarctic ice sheet: lessons from Foundation Ice Stream: Annals of Glaciology, p. 1–6, doi: 10.1017/aog.2017.9.

Jakobsson, M., Nilsson, J., Anderson, L., Backman, J., Björk, G., Cronin, T. M., Semiletov, I., 2016, Evidence for an ice shelf covering the central Arctic Ocean during the penultimate glaciation. Nature Communications, 7, 10365. http://doi.org/10.1038/ncomms10365

Jamieson, S.S.R.R., Vieli, A., Livingstone, S.J., Cofaigh, C.Ó., Stokes, C., Hillenbrand, C.-D., Dowdeswell, J. a., Ó Cofaigh, C., Stokes, C., Hillenbrand, C.-D., and Dowdeswell, J. a., 2012, Ice-stream stability on a reverse bed slope: Nature Geoscience, v. 5, p. 799–802, doi: 10.1038/NGEO1600.

Jezek, K.C., and Bentley, C.R., 1983, Field studies of bottom crevasses in the Ross Ice Shelf, Antarctica: Journal of Glaciology, v. 29, p. 118–126.

Joughin, I., Tulaczyk, S., Bindschadler, R., and Price, S.F., 2002, Changes in west Antarctic ice stream velocities: Observation and analysis: Journal of Geophysical Research: Solid Earth, v. 107, p. EPM 3-1-EPM 3-22, doi: 10.1029/2001JB001029.

Joughin, I., Abdalati, W., and Fahnestock, M., 2004, Large fluctuations in speed on Greenland's Jakobshavn Isbræ glacier: Nature, v. 432, p. 608–610, doi: 10.1038/nature03130.

Klages, J.P., Kuhn, G., Hillenbrand, C.D., Graham, A.G.C., Smith, J.A., Larter, R.D., Gohl, K., and Wacker, L., 2014, Retreat of the West Antarctic Ice Sheet from the western Amundsen Sea shelf at a pre- or early LGM stage: Quaternary Science Reviews, v. 91, p. 1–15, doi: 10.1016/j.quascirev.2014.02.017.

Larter, R.D., Anderson, J.B., Graham, A.G.C., Gohl, K., Hillenbrand, C.D., Jakobsson, M., Johnson, J.S., Kuhn, G., Nitsche, F.O., Smith, J.A., Witus, A.E., Bentley, M.J., Dowdeswell, J.A., Ehrmann, W., et al., 2014, Reconstruction of changes in the Amundsen Sea and Bellingshausen Sea sector of the West Antarctic Ice Sheet since the Last Glacial Maximum: Quaternary Science Reviews, v. 100, p. 55–86, doi: 10.1016/j.quascirev.2013.10.016.

Le Meur, E., Sacchettini, M., Garambois, S., Berthier, E., Drouet, A.S., Durand, G., Young, D., Greenbaum, J.S., Holt, J.W., Blankenship, D.D., Rignot, E., Mouginot, J., Gim, Y., Kirchner, D., et al., 2014, Two independent methods for mapping the grounding line of an outlet glacier - An example from the Astrolabe Glacier, Terre Adélie, Antarctica: Cryosphere, v. 8, p. 1331–1346, doi: 10.5194/tc-8-1331-2014.

Lowe, A.L., and Anderson, J.B., 2002, Reconstruction of the West Antarctic ice sheet in Pine Island Bay during the Last Glacial Maximum and its subsequent retreat history: Quaternary Science Reviews, v. 21, p. 1879–1897.

Matsuoka, K., Hindmarsh, R.C.A., Moholdt, G., Bentley, M.J., Pritchard, H.D., Brown, J., Conway, H., Drews, R., Durand, G., Goldberg, D., Hattermann, T., Kingslake, J., Lenaerts, J.T.M., Martín, C., et al., 2015, Antarctic ice rises and rumples: Their properties and significance for ice-sheet dynamics and evolution: Earth-Science Reviews, v. 150, p. 724–745, doi: 10.1016/j.earscirev.2015.09.004.

Mosola, A.B., and Anderson, J.B., 2006, Expansion and rapid retreat of the West Antarctic Ice Sheet in eastern Ross Sea: possible consequence of over-extended ice streams? Quaternary Science Reviews, v. 25, p. 2177–2196, doi: 10.1016/j.quascirev.2005.12.013.

Pandey, D., Chaubey, A., and Rajan, S., 2008, Seismic imaging of glaciomarine sediments of Antarctica: Optimizing the acquisition parameters: Indian Journal of Marine Sciences, v. 37, p. 412–418.

Parizek, B.R., and Alley, R.B., 2004, Ice thickness and isostatic imbalances in the Ross Embayment, West Antarctica: Model results: Global and Planetary Change, v. 42, p. 265–278, doi: 10.1016/j.gloplacha.2003.09.005.

Peltier, W.R., and Fairbanks, R.G., 2006, Global glacial ice volume and Last Glacial Maximum duration from an extended Barbados sea level record: Quaternary Science Reviews, v. 25, p. 3322–3337, doi: 10.1016/j.quascirev.2006.04.010.

Ross, N., Bingham, R.G., Corr, H.F.J., Ferraccioli, F., Jordan, T.A., Le Brocq, A., Rippin, D.M., Young, D., Blankenship, D.D., and Siegert, M.J., 2012, Steep reverse bed slope at the grounding line of the Weddell Sea sector in West Antarctica: Nature Geoscience, v. 5, p. 393–396, doi: 10.1038/ngeo1468.

Shipp, S., Anderson, J., and Domack, E., 1999, Late Pleistocene-Holocene retreat of the West Antarctic Ice-Sheet system in the Ross Sea: Part 1 - Geophysical results: Bulletin of the Geological Society of America, v. 111, p. 1486–1516, doi: 10.1130/0016-7606(1999)111<1486.

Weertman, J., 1974, Stability of the junction of an ice sheet and an ice shelf: Journal of Glaciology, v. 13, p. 3–11, doi: 10.3198/1974JoG13-67-3-11.

Wellner, J. S., A. L. Lowe, S. S. Shipp, and Anderson, J. B., 2001, Distribution of glacial geomorphic features on the Antarctic continental shelf and correlation with substrate: Implications for ice behavior, Journal of Glaciology, v. 47, p. 397– 411.

Whillans, I.M., and Van der Veen, C.J., 1997, The role of lateral drag in the dynamics of Ice stream B, Antarctica, Journal of Glaciology., v. 43, p. 231–237.

Whitehouse, P.L., Bentley, M.J., and Le Brocq, A.M., 2012, A deglacial model for Antarctica: Geological constraints and glaciological modelling as a basis for a new model of Antarctic glacial isostatic adjustment: Quaternary Science Reviews, v. 32, p. 1–24, doi: 10.1016/j.quascirev.2011.11.016.

APPENDIX. SUPPLEMENTAL DATA

Supplementary Table 1. Results of calculation of minimum ice thickness using grounding line positions on the seismic line 1502b-03, the time record from DeCesare et al., (in prep.), and the eustatic sea level curve from Peltier and Fairbanks (2006)

Time (kyrs before present)	Position	Sea level correction from Peltier and Fairbanks (m)	Present-day Water Depth (mbsl) at the paleo grounding line	Paleo Water Depth, z_g (mbsl)	Estimated paleo-Ice Thickness at grounding line, H_g (m)
18	LGM	-112	623.43	511.43	584.1667111
17.1	GL 1	-110	620	510	582.5333333
15.9	GL 2	-107	614.06	507.06	579.1752
14.7	GL 3	-94	600	506	577.9644444
13.5	GL 4	-71	595	524	598.5244444
12.3	GL 5	-60	567.19	507.19	579.3236889
12	GL 6	-55	557.809	502.809	574.3196133
11.7	GL 7	-53	534.4	481.4	549.8657778
11.5(pre-retreat)	Top of GZW 7	-51	492.18	441.18	503.9256
11.5(post-retreat)	GL 8	-51	586	535	611.0888889

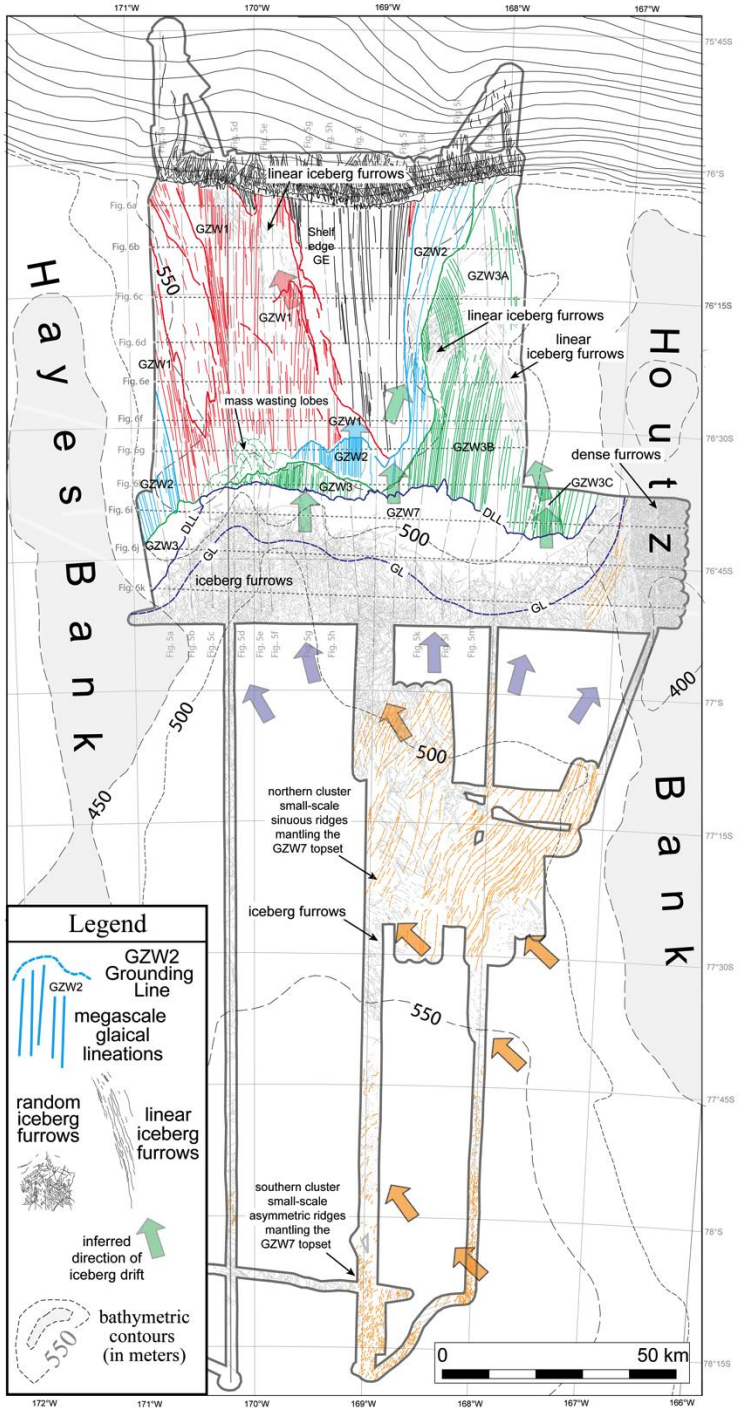

Supplemental Figure 1: GZW, grounding line and other geomorphic features as interpreted from multibeam bathymetry collected on the outer and middle-shelf of Whales Deep. The grounding lines interpreted from the multi-beam were used to guide the interpretations of the Brown Unconformity reconstruction map (from Bart et al., 2017a).

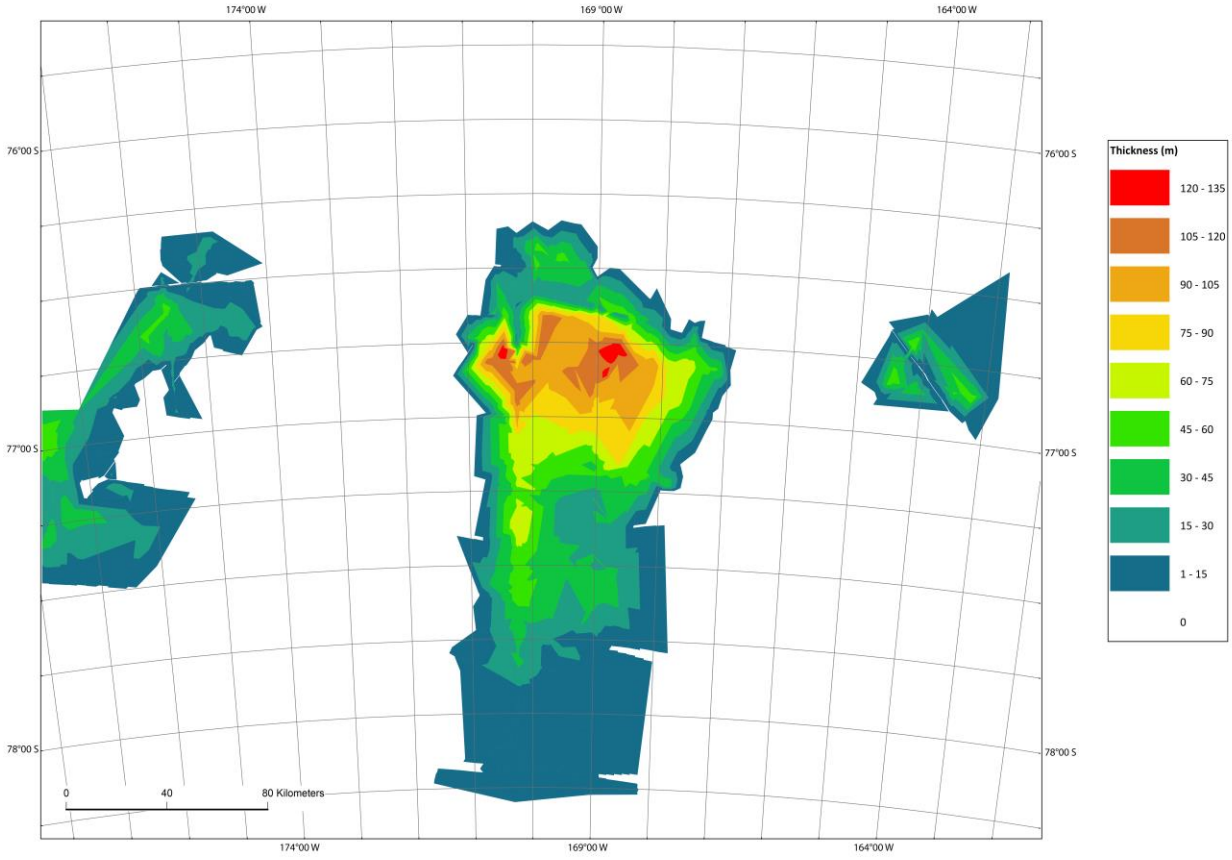

Supplemental Figure 2: Isopach subtraction map created by subtracting the Brown Unconformity TIN from the Seafloor TIN using the ArcGIS software. This process yields a thickness map of the post-LGM sediment. The areas of the map with no post-LGM thickness are the regions where the Brown Unconformity is the seafloor reflection because there is not post-LGM sediment. This mostly coincides with the banks of the trough and illustrates the post-LGM GZW cluster as trough confined.

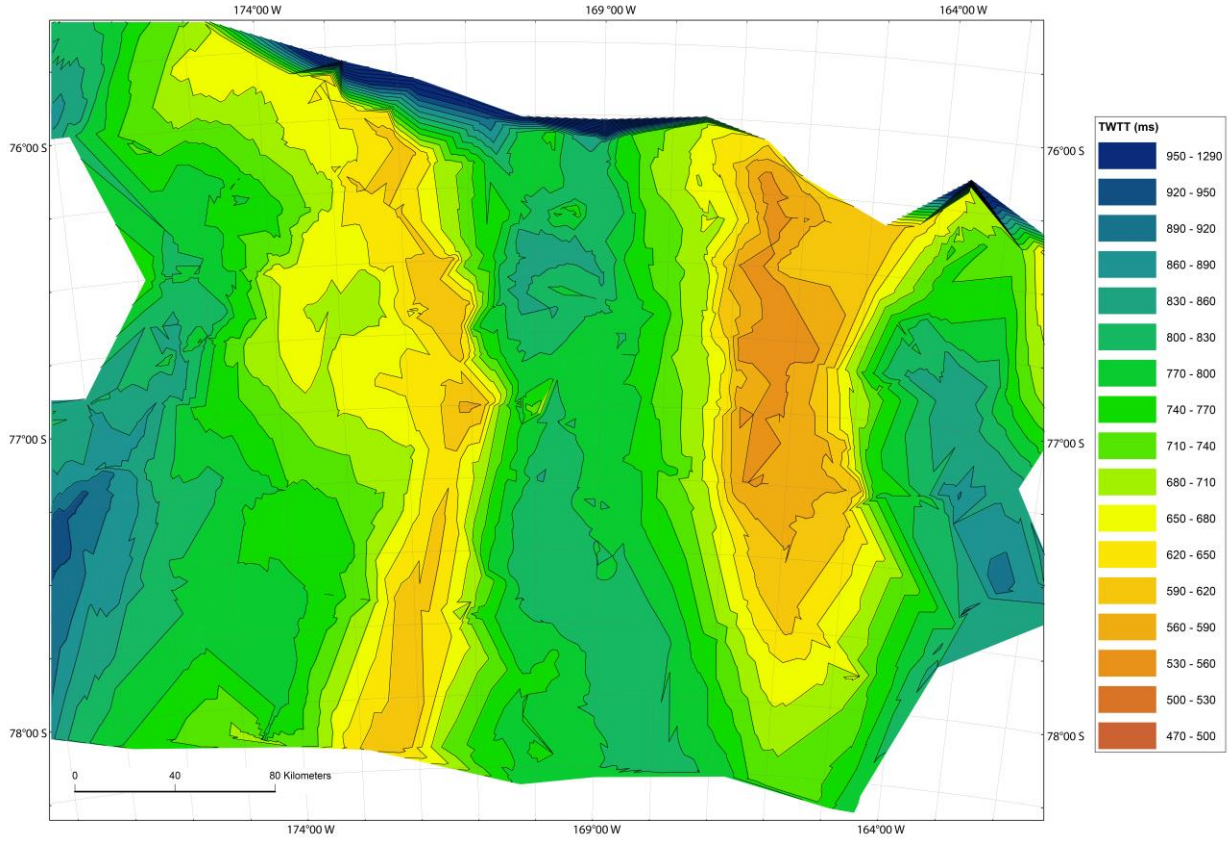

Supplemental Figure 3: Two-way travel time TIN created for the Brown Unconformity. The shown topography is from the seismic lines and is un-depth converted.

VITA

Matthew Danielson, from Houston, Texas, graduated from Strake Jesuit College Preparatory in 2011. He then attended and graduated from Texas A&M University with a Bachelor of Science in Geology in December of 2015. Matthew then entered graduate school at Louisiana State University and plans to graduate in May of 2018. Upon graduating from LSU, Matthew seeks to work as geologist in the oil and gas industry.